SPITZER OBSERVATIONS OF EXOPLANETS DISCOVERED WITH THE KEPLER K2 MISSION

Item Type	Article
Authors	Beichman, Charles; Livingston, John; Werner, Michael; Gorjian, Varoujan; Krick, Jessica; Deck, Katherine; Knutson, Heather; Wong, Ian; Petigura, Erik; Christiansen, Jessie; Ciardi, David; Greene, Thomas P.; Schlieder, Joshua E.; Line, Mike; Crossfield, Ian; Howard, Andrew; Sinukoff, Evan
Citation	SPITZER OBSERVATIONS OF EXOPLANETS DISCOVERED WITH THE KEPLER K2 MISSION 2016, 822 (1):39 The Astrophysical Journal
DOI	10.3847/0004-637X/822/1/39
Publisher	IOP PUBLISHING LTD
Journal	The Astrophysical Journal
Rights	© 2016. The American Astronomical Society. All rights reserved.
Download date	10/08/2022 06:00:06
Item License	http://rightsstatements.org/vocab/InC/1.0/
Version	Final published version
Link to Item	http://hdl.handle.net/10150/621243

SPITZER OBSERVATIONS OF EXOPLANETS DISCOVERED WITH THE KEPLER K2 MISSION

CHARLES BEICHMAN[1], JOHN LIVINGSTON[2], MICHAEL WERNER[2], VAROUJAN GORJIAN[2], JESSICA KRICK[3], KATHERINE DECK[4],
HEATHER KNUTSON[4], IAN WONG[4], ERIK PETIGURA[4], JESSIE CHRISTIANSEN[5], DAVID CIARDI[5], THOMAS P. GREENE[6],
JOSHUA E. SCHLIEDER[6], MIKE LINE[7], IAN CROSSFIELD[8,10], ANDREW HOWARD[9], AND EVAN SINUKOFF[9]

[1] NASA Exoplanet Science Institute, California Institute of Technology, Jet Propulsion Laboratory, Pasadena, CA 91125, USA
[2] Jet Propulsion Laboratory, California Institute of Technology, Pasadena, CA 91125, USA
[3] Infrared Processing and Analysis Center, California Institute of Technology, Pasadena, CA 91125, USA
[4] California Institute of Technology, Pasadena, CA 91125, USA
[5] NASA Exoplanet Science Institute, California Institute of Technology, Pasadena, CA 91125, USA
[6] NASA Ames Research Center, Mountain View, CA 94035, USA
[7] University of California, Santa Cruz, Santa Cruz, CA 95064, USA
[8] University of Arizona, Tucson, AZ 85721, USA
[9] Institute for Astronomy, University of Hawaii, Honolulu, HI 96822, USA

ABSTRACT

We have used the *Spitzer Space Telescope* to observe two transiting planetary systems orbiting low-mass stars discovered in the *Kepler K2* mission. The system K2-3 (EPIC 201367065) hosts three planets, while K2-26 (EPIC 202083828) hosts a single planet. Observations of all four objects in these two systems confirm and refine the orbital and physical parameters of the planets. The refined orbital information and more precise planet radii possible with *Spitzer* will be critical for future observations of these and other *K2* targets. For K2-3b we find marginally significant evidence for a transit timing variation between the *K2* and *Spitzer* epochs.

Key words: planets and satellites: dynamical evolution and stability – planets and satellites: gaseous planets

1. INTRODUCTION

1.1. Demographics and Properties of Planets Orbiting M Stars

One of the primary goals of the repurposed *Kepler* spacecraft (the "*K2* mission") is a wider survey of late-type stars than was achieved within the primary *Kepler* mission (Beichman et al. 2013; Howell et al. 2014). Population studies of the *Kepler* data suggest an increased incidence of lower-mass planets orbiting M stars (Howard et al. 2012). Although *Kepler* observed only about 3000 M stars, initial results suggest a high incidence of planets orbiting low-mass stars, approaching 100% (Dressing & Charbonneau 2013, 2015), of which up to 25% may reside in the loosely defined stellar habitable zone (HZ; Dressing & Charbonneau 2015). These effects must be explained in the context of planet formation theory (Payne & Lodato 2007; Mordasini et al. 2012) and make the validation of these trends with a larger sample of great interest. By surveying a dozen or more fields, each containing ~4000 late-type stars, *K2* promises to increase the sample of M star planetary systems more than 10-fold.

Planets orbiting M stars are important for reasons beyond their demographics. Because cool stars have smaller radii than earlier spectral types, the transit signal of a given sized planet is proportionately larger, resulting in easier follow-up spectroscopic observations with the *Hubble Space Telescope* (*HST*; Knutson et al. 2014) and, soon, the *James Webb Space Telescope* (*JWST*; Beichman et al. 2014). While an Earth analog (1 $R_\oplus$) orbiting a solar-type star in a 1 au HZ produces a 84-part-per-million (ppm) transit signal every 365 days, the same planet orbiting in the HZ of an M3 star produces a >500 ppm signal every ~30 days. Thus, *JWST* spectroscopy will be able to probe down to at least the super-Earth level (Batalha et al. 2014) for late-type stars. Stellar brightness is

another critical parameter for transit spectroscopy. In this regard, *K2* offers an advantage over *Kepler* by covering ~10 times more sky, so that with careful selection it will be possible to target M stars that are 1–2 mag brighter than those in *Kepler*'s primary field. Eventually, the *TESS* mission, with its all-sky coverage, will gain an average of 3–5 mag in host star brightness over *Kepler* (Ricker et al. 2014; Sullivan et al. 2015).

Numerous groups have proposed M star candidates for *K2* and are engaged in follow-up activities to identify, validate, and characterize candidates found in the *K2* light curves. In this paper we introduce a follow-up effort using the *Spitzer Space Telescope* to improve the orbital ephemerides and other properties of *K2* planets hosted by cool stars. We report the results for two systems: K2-3, an M0 star with three planets (EPIC 201367065b, c, d; Crossfield et al. 2015), and K2-26 (EPIC 202083828), an M1 star with a single transiting planet (Schlieder et al. 2016).

1.2. The Spitzer K2 Transit Program

A proposal to follow up planets hosted by M stars by *K2* using *Spitzer* observations at 4.5 μm (IRAC Channel 2) was approved in Cycle 11 (Werner, PI; Program 11026). *Spitzer* observations will augment and complement *K2* results in a number of important ways.

1. *Kepler*'s 30-minute observing cadence means that the ingress and egress of a transit or even the entire transit, which might be as short as 1 hr for a late M star, will have only a handful of *Kepler* samples per event. For comparable signal-to-noise ratio (S/N) on the transit depth, *Spitzer* transits provide much tighter constraints on the orbital and system parameters because of the much finer sampling (0.4–30 s versus 30 minutes for *K2*).

---
[10] NASA Sagan Fellow.

2. By observing 1 yr or more after *K2*'s measurements, *Spitzer* in conjunction with the original *K2* results can dramatically improve the orbital ephemerides and thus enable accurate predictions of transit timing many years into the future, which will be particularly important for *JWST* observations. In the case of multiple systems, *Spitzer* may reveal transit timing variations (TTVs), which may be used to estimate planetary masses.

3. M stars show strong limb darkening in the *Kepler* bandpass, which complicates the determination of the transit parameters and the planetary characteristics. Much less limb darkening is present in the *Spitzer* 3.6 and 4.5 um bands (Claret & Bloemen 2011). Thus, the *Spitzer* measurements permit a much cleaner determination of the transit parameters, particularly given the sampling issue discussed above.

4. To first order, the depth of a transit should be achromatic. This lack of change of transit depth with wavelength means that *Spitzer* results can be used to reject certain false-positive alternatives to the transit interpretation, e.g., a low-mass stellar companion, particularly in the absence of radial velocity observations. There are, however, small wavelength-dependent variations between the visible and infrared that may be interpreted in terms of atmospheric structure, e.g., the presence of molecular absorptions or a temperature inversion. Such claims are at the limits of *Spitzer*'s accuracy (Evans et al. 2015; Wong et al. 2015).

5. Two additional advantages of *Spitzer*, a lower level of photospheric noise ("stellar jitter") in the infrared compared with visible wavelengths, and the detection of secondary eclipses for hot, short-period planets, may eventually be demonstrated on M stars still to be identified by *K2*.

Taking the above considerations into account, *Spitzer* provides an important means of screening M star exoplanets and identifying those most promising for *JWST* follow-up, especially because IRAC spans the middle of *JWST*'s spectro-scopic wavelength range. The results presented herein will demonstrate the value of *Spitzer* in all of these areas. The approved *Spitzer* program will observe of order 30 transiting systems with over 450 hr of telescope time with the goal of improving planetary and orbital properties for the brightest, most promising targets for future spectroscopic follow-up.

1.3. The Need for Improved Ephemerides

A focus of this paper will be the importance of *Spitzer* observations to improve significantly the ability to recover future transits. At the simplest level, the ability to predict the time of a future transit, $T(n)$, depends on the uncertainty in the reference time for an initial mid-transit time, $\sigma(T_0)$, and the uncertainty in the orbital period, σP, projected n orbits into the future:

$$T(n) = T_0 + nP \tag{1}$$

and

$$\sigma(T_n) = \sqrt{\sigma(T_0)^2 + (n\sigma(P))^2}. \tag{2}$$

Equation (2) shows that the uncertainty in the mid-transit time increases linearly with orbit number after the reference orbit. Thus, for example, for the planet K2-3d (see Table 1) *K2*

data alone yield T_0 (BJD) = 2,456,826.2233 ± 0.0039 (2014 June 17) and $P = 44.5629 ± 0.0057$. By the time *JWST* gets around to observing this object on, say, BJD 2,458,817.609 (2019 December 14), 45 orbits after its initial observation by *K2*, the 1σ uncertainty in the transit midpoint would be ∼6 hr. Such a large uncertainty would increase the duration required for a *JWST* observation by ∼12 hr (from -1σ to $+1\sigma$) relative to a short 4 hr transit to be sure of capturing the entire transit at even the 1σ level. As we demonstrate in this paper, the addition of even a single *Spitzer* observation can reduce this uncertainty by a factor of 5–10.

2. OBSERVED TARGETS

The first two objects we observed with *Spitzer* came from early discoveries from *K2* in Fields 0 and 1.[11]

The multiple system K2-3 (EPIC 201367065) has three planets orbiting an M0 star (Crossfield et al. 2015) as described in Table 1. The three planets (b, c, d) have radii in the range of 1.2–2.4 $R_\oplus$ and were observed by *K2* with eight, four, and two transits, respectively. The star is bright in near-IR wavelengths ($K_s = 8.56$ mag, Skrutskie et al. 2006; *WISE* [4.6] = 8.42 mag, Wright et al. 2010), with a radius of 0.56 ± 0.068 $R_\odot$, making it a promising target for *JWST* follow-up, which requires bright targets for high-S/N spectroscopy. The outermost planet, K2-3d, is in the nominal HZ with an insolation of 1.5 ± 0.5 times Earth's and an effective temperature around 300 K (Crossfield et al. 2015).

Examination of the sources in the Campaign 0 field led to the identification of a 2.7 $R_\oplus$ planet with an effective temperature of <500 K orbiting the M1 star K2-26 ($K_s = 10.53$ mag; *WISE* [4.6] = 10.35 mag) on a 14.5-day period. As described in Schlieder et al. (2016), the host star is an M1.0 ± 0.5 dwarf with near-solar metallicity, [Fe/H] = −0.13 ± 0.15, and a stellar radius of 0.52 ± 0.08 $R_\odot$. Schlieder et al. (2016) argue that from the examination of HIRES spectroscopy, which rules out spectroscopic binaries earlier than M4.5 V, LBT/LMIRcam and Robo-AO adaptive optics imaging, and archival survey images spanning more than 50 yr, the likelihood of this planet candidate being a false positive owing to an eclipsing binary or hierarchical multiple system is extremely small. Thus, we included this object in our *Spitzer* program.

3. *SPITZER* DATA AND ANALYSIS

In 2015 March K2-3b was observed by *Spitzer* on two epochs, while planets "c" and "d" were observed once each. All three were observed one more time, each approximately 6 months later in 2015 September (Table 2). K2-26b was observed once in 2015 March. The science observations were timed to begin 2 hr before the start of the transit and end 2 hr after the end of the transit to allow adequate baseline on either side of the event. We preceded the main observation with a 30-minute pre-observation of the target to mitigate the effect of large drifts across the pixel due to temperature changes in the spacecraft after large slews from the preceding observations (Grillmair et al. 2012).

All observations were obtained with *Spitzer* IRAC Channel 2 (4.5 μm; Fazio et al. 2004; Werner et al. 2004) using staring mode observations. We choose Ch2 because the dominant instrumental systematic of changing gain as a function of

---

[11] http://keplerscience.arc.nasa.gov/k2-fields.html

Table 1
Properties of *K2* Stars and Planets

Star Name/Position	Spec Type	*Kepler* Mag (mag)	K_s (mag)	Planet	R_{pl} ($R_\oplus$)	R_{pl}/R_*	Period (days)
K2-3 (1)	M0 ± 0.5	11.57	8.56	b	2.14 ± 0.27	$0.0348^{+0.0012}_{-0.0007}$	10.05402 ± 0.00026
EPIC 201367065				c	1.72 ± 0.23	$0.027^{+0.0014}_{-0.0008}$	24.6454 ± 0.0013
$11^h29^m20^s49$ $-01°27'18''4$ (J2000,Epoch 2015.7)[a]				d	1.52 ± 0.20	$0.025^{+0.0014}_{-0.0017}$	44.5629 ± 0.0057
K2-26 (2)	M1.0 ± 0.5	12.47	10.53	b	$2.67^{+0.46}_{-0.42}$	$0.0471^{+0.0037}_{-0.0021}$	$14.5665^{+0.0016}_{-0.0020}$
$06^h16^m49^s55$ $+24°35'45''0$ (J2000, Epoch 2015.7)[a]							

Note.
[a] The positions of both stars were corrected for proper motion from Epoch 2000 to the date of observation using positional data from the *WISE* survey and Two Micron All Sky Survey.
References. (1) Crossfield et al. 2015; (2) Schlieder et al. 2016.

Table 2
Spitzer Observing Log

Planet Name	*Spitzer* Duration (hr)	Exposure Time (s)	Observing Date (UT)
K2-3b	7.0	2	2015 Mar 13
K2-3b	7.0	2	2015 Mar 23
K2-3c	7.9	2	2015 Mar 26
K2-3d	8.5	2	2015 Mar 11
K2-3b	7.0	2	2015 Sep 10
K2-3c	7.9	2	2015 Sep 15
K2-3d	8.5	2	2015 Sep 06
K2-26b	7.4	12	2015 Mar 12

position is a smaller effect in Ch2 than in Ch1 (Ingalls et al. 2012); the diminished effect of limb darkening in Ch2 is also advantageous. Staring mode is standard practice for exoplanet observations in order to keep the star on one position within a single pixel. To ensure that the most well-calibrated position with minimal gain variation is achieved on the pixel, a peak-up star was used to place the target star (corrected for proper motion; Table 1) on the "sweet spot" of the central pixel. Exposure times were chosen to maintain the well depth in the linear regime of the detector. K2-3 was observed in subarray mode with 2 s frame times, and K2-26b was observed with 12 s exposures in full array mode. The same "sweet spot" was used for both stars. This observing strategy resulted in over 53,928 individual photometry points used in the analysis described below.

3.1. Photometric Analysis

Centroiding and aperture photometry were performed using the Python package *photutils*. Aperture photometry was computed for each exposure using radii ranging from 2.0 to 2.9 pixels in 0.1 pixel increments, as well as 3.0–5.0 pixels in 0.5 pixel increments. Optimal photometric radii were determined for each data set by choosing the time series with minimal scatter, thus minimizing the contribution from background noise while including enough of stellar flux to maximize S/N. The typical radius values used were 2.2 or 2.3 pixels, which is consistent with independent analysis of optimal *Spitzer* transit photometry (Krick et al. 2015). Sky background levels and photometric uncertainties were computed taking into account known characteristics of the detector. Because of the small size (32 × 32 pixels) of subarray images, this estimate entails a trade-off between good number statistics

and contamination from the stellar point-spread function (PSF). We approached this by fitting a Gaussian to each frame after masking pixels within the central PSF and central two rows and columns, as well as the top row, which is systematically biased to lower values (see Knutson et al. 2012 for more detailed discussion).

3.2. Spitzer *Systematics*

The largest systematic in *Spitzer* photometry arises from intrapixel gain variations. Spacecraft-induced motion, coupled with an undersampled PSF, leads to measured flux variations of order a few percent (Ingalls et al. 2012). The spacecraft motions are of several types: variable-duration thermal settling of the spacecraft, pointing control errors resulting in long-term drift, a 39-minute sawtooth pointing oscillation due to the cycling of a battery heater in the spacecraft bus, as well as both high- and low-frequency jitter due to a variety of possible causes, including harmonic coupling of the reaction wheel assembly to the spacecraft structure (Grillmair et al. 2012).

We used the pixel-level decorrelation (PLD) method technique (Deming et al. 2015) to reduce these systematic photometric variations. Similar to Deming et al. (2015), we fit the PLD pixel coefficients simultaneously with a temporal systematic model. We opt for a linear (instead of quadratic) ramp in time because the data do not obviously warrant the increase in model complexity, and a quadratic ramp is more likely to be degenerate with the transit signal. Thus, the total deviation in signal at time t is modeled as

$$\Delta S^t = \sum_{i=1}^{N} c_i \hat{P}_i^t + T(t) + mt + b, \qquad (3)$$

where the c_i are the coefficients that represent the partial derivatives from the Taylor expansion described by Deming et al. (2015), $T(t)$ is the transit signal, and m and b are the coefficients of the linear ramp in time. $\hat{P}_i^t$ is the ith pixel value of the normalized pixel grid at time t:

$$\hat{P}_i^t = \frac{P_i^t}{\sum_{i=1}^{N} P_i^t}. \qquad (4)$$

We tried using both a 3 × 3 and a 5 × 5 pixel grid centered on the target, and we found that while a 3 × 3 grid produced good results, a 5 × 5 grid further reduced the residual rms at minimal computational cost. We took an iterative approach to fitting the systematic coefficients, which allows for a gradual

refinement due to intermediate improvements in the estimate of the nonsystematic signal, i.e., the transit. We fit the systematic coefficients while the transit parameters are held fixed, then fit for the transit parameters while the systematic coefficients are held fixed, and repeat until a convergence criterion is met. At each iteration the parameters are updated with their new maximum likelihood estimate (MLE) values using the Nelder–Mead simplex algorithm and a Gaussian likelihood.

Because the transit depths of these planets are in some cases (K2-3d) approaching the limit of *Spitzer*'s precision, simultaneous fitting of the systematic and astrophysical parameters can lead to the nonconvergence of a wide variety of numerical optimization algorithms. Initial testing showed that a modest improvement in the estimate of the systematic component prior to fitting any transit parameters prevented this, which led to the development of the iterative approach described above. This is perhaps due to operating near the limit of the instrument capability, combined with degeneracies between transit and systematic parameters that complicate the objective function. For example, tests conducted with higher-S/N *Spitzer* transit data in which the amplitude of the systematic signals is smaller compared to the transit signal transit depth do not exhibit the same difficulty. However, this effect is mitigated by operating on unbinned data, and the transit parameter estimates derived from the *K2* data are of sufficient quality.

3.3. Transit Fitting and Derived Parameters

In the context of the above discussion, one possible drawback of this iterative method in lower-S/N data sets is an increased reliance on good starting guesses for the transit parameters, as these are held fixed while the initial PLD coefficients are fit. Although variation of bin size typically resulted in a tight range of fitted transit parameters, in some cases larger bin sizes resulted in increased sensitivity to initial parameter estimates. Testing with unbinned data showed that the sensitivity to initial parameter estimates is typically about two orders of magnitude smaller than the uncertainties derived from the final posteriors. Thus, in order to be more robust to uncertainties in the initial transit parameters, and because of the relatively low computational complexity of PLD, we analyzed the data without binning. Furthermore, although we typically detect no significant correlated noise (at 95% confidence) after PLD, even low levels of residual correlation could induce biases in fits to the binned data. The iterative approach described above typically adds only minor additional complexity, so the bulk of the total computation cost is expended during the sampling of transit parameter posterior distributions.

For transit parameter estimates and uncertainties, we use the open-source *emcee* package (Foreman-Mackey et al. 2013), an efficient Python implementation of the affine-invariant Markov Chain Monte Carlo (MCMC) ensemble sampler (Goodman & Weare 2010). To fit the PLD-corrected data produced by the iterative method described above, we use the open-source PyTransit code (Parviainen 2015) to generate the transit model. For the planets of K2-3 we take a conservative approach to fitting the astrophysical parameters by using wide flat priors on the mid-transit time, scaled semimajor axis, inclination, and planet-to-star radius ratio. This produced fairly Gaussian posteriors for all parameters except the scaled semimajor axis, which has a distinctly skewed posterior owing to degeneracy with the inclination parameter. For K2-26b we use Gaussian priors set by the values reported by Schlieder et al. (2016),

because the egress of the transit in the *Spitzer* data was too close to being missed to ensure good fits using flat priors. We ensured that the MCMC chains produced by the sampler were of sufficient quality by monitoring both the autocorrelation time and the acceptance fraction, as well as by visual inspection of the chains and corner plots of the posteriors.

The results of the correction of the *Spitzer* photometry to reveal the transit signals are shown in Figure 1. The derived system parameters are given in Table 3.

4. RESULTS AND DISCUSSION

4.1. Comparison of K2 and Spitzer Parameters

The fundamental transit parameters of period and depth are consistent between the *K2* and *Spitzer* data sets. Consider the case of K2-3b, for which the *Spitzer* data alone yield a period of 10.054440 ± 0.0000053 days, which can be compared with the *K2*-only value of 10.05402 ± 0.00026 days (Crossfield et al. 2015), which differ from one another by 1.6σ. By combining the individual *K2* and *Spitzer* transit times simultaneously, we obtain a new, more accurate period (Crossfield et al. 2015 and Table 3) of 10.0545435 ± 0.000029 days (Table 4), which differs from the *K2*-only value by 2σ. We discuss the apparent difference between the two estimates below in a discussion of possible TTVs in Section 4.2.

In Table 4 and Figure 2 we present combined period estimates that represent a 5- to 10-fold improvement due to the longer temporal baseline in the combined data sets. Using these new values *and assuming no TTVs*, we can project the ephemerides of K2-3b, c, d into the *JWST* era (circa 2019 December) to be less uncertain than 0.11, 0.28, and 0.40 hr, respectively, compared with *K2*-only uncertainties of 1.3, 2.5, and 6 hr. These results show the importance of *Spitzer* observations in greatly reducing the uncertainties in transit times for future observations.

The other parameter of primary importance is the depth of the transit, or the derived parameters R_p/R_* and $R_p/R_\oplus$. These are very similar between the *K2*-only and *K2-Spitzer* values for all four planets. As shown in Tables 1 and 3, the differences in the transit depths are within 1σ, with refined values given in Table 5. In the case of K2-26b it is important to note that the close similarity in transit depth provides further confidence in the planetary nature of the transiting source. False positives due to an eclipsing binary or hierarchical system would have a markedly different eclipse depth in the *Spitzer* band (Désert et al. 2015).

4.2. Transit Timing

Deviations from the transit times predicted by a constant-period (Keplerian) orbit can be indicative of mutual gravitational interactions between planets. TTVs have proven to be an important method of validating *Kepler* planets and measuring dynamical masses (e.g., Carter et al. 2012; Steffen et al. 2013).

With the longer baseline allowed by *Spitzer*, we examined the central transit times for the K2-3 system to assess the statistical significance of any TTVs. In addition to measuring the transit times of the transits observed with *Spitzer* (Table 6), we obtained *K2* light curves for all of the individual K2-3 transit events (Crossfield et al. 2015), which allows us to fit individual transit times (Table 6) for the planets of K2-3 in the original *K2* observing campaign. Note, however, that for any
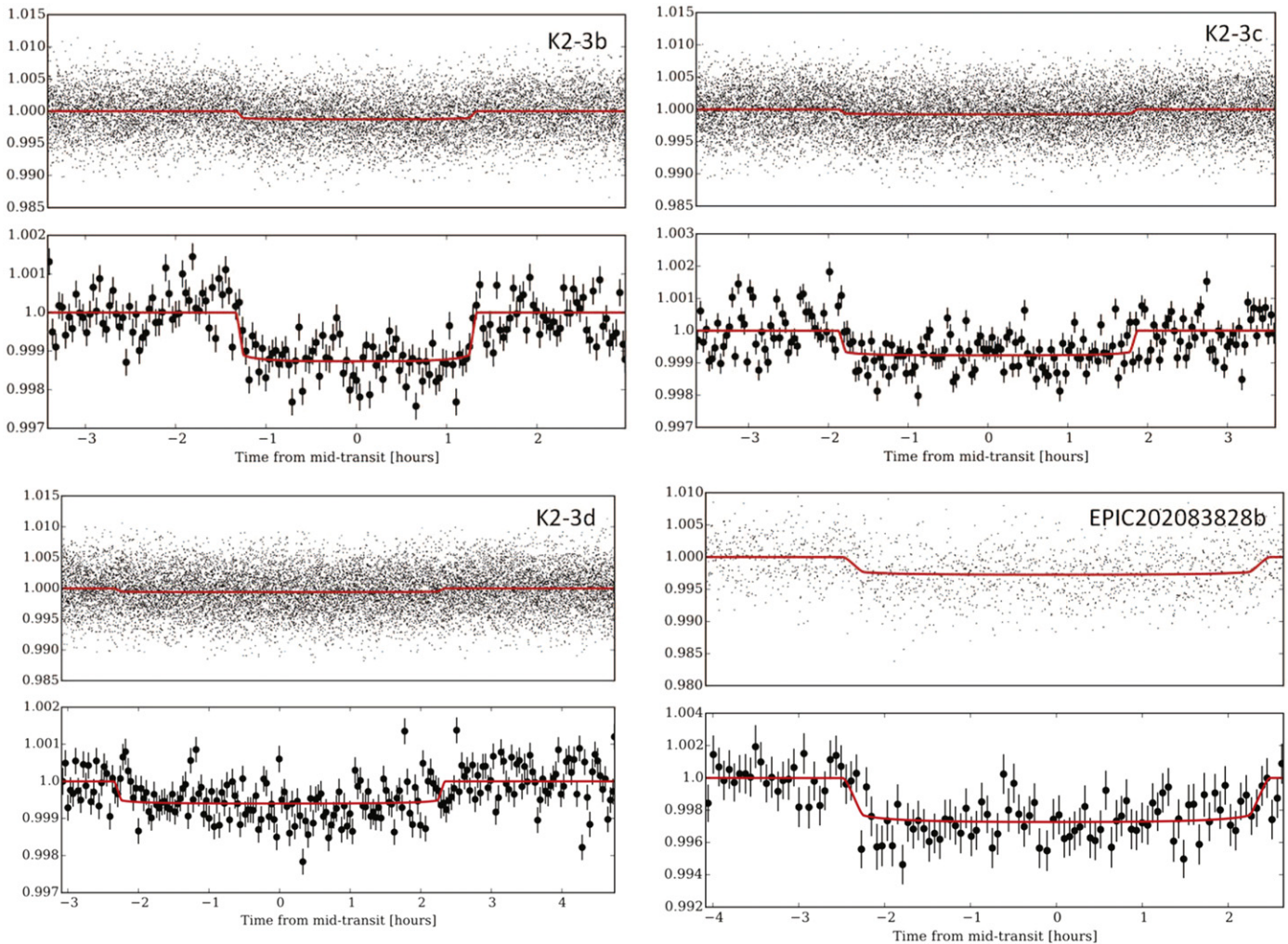
Figure 1. Calibrated light curves for the four planets shown as normalized flux as a function of time from mid-transit. The top plot of each of the four panels shows unbinned fluxes, and the bottom plot shows binned fluxes, both PLD corrected as described in the text. Red lines are the best-fit models. Note the Y-axis change from unbinned to binned plots. Transit fits to *Spitzer* data from 2015 March are as described in the text. Top left: planet K2-3b; top right: planet K2-3c; bottom left: planet K2-3d; bottom right: planet EPIC20203828b.

individual *K2* transit there are only a handful of individual data points with which to fit each transit, with the result that the individual timing uncertainties are large, e.g., ±2.5 minutes.

While the *K2* transit times for K2-3b alone are consistent with a constant-period model (which is in turn consistent with the mean ephemeris reported by Crossfield et al. 2015), the combined *Spitzer* and *K2* data set shows some evidence of TTVs. When all 11 data points are considered, the deviation from a constant-period model is statistically significant with a χ^2 of 23 for 9 degrees of freedom. Visual inspection of the individual *K2* transit times of K2-3b suggests a coherent variation of ∼±5 minutes relative to the mean period estimated from the combined data set (data points shown in red in the lower panel labeled "b" in Figure 3). However, the major contributor to the χ^2 is the *Spitzer* data, which suggest the existence of a TTV with an amplitude around 2 ± 1 minutes. The individual transit times for the combined *K2*+*Spitzer* data for the outer two planets are consistent with constant-period orbits (data points shown in red in the lower panel of Figure 3) with $\chi^2 = 3.4$ and 1.4, with 4 and 2 degrees of freedom, respectively.

We consider briefly the amplitude of the TTVs one might expect for the K2-3 system in one representative configuration

with very nearly circular orbits, a mass for K2-3b of ∼8 $M_{\oplus}$ (Almenara et al. 2015), and masses of 5 $M_{\oplus}$ for the outer two planets (based roughly on the mass–radius relationship in Weiss & Marcy 2014). Illustrative TTVs for "b" and the outer two planets in this configuration calculated using the code *TTVFast* (Deck et al. 2014) are shown in Figure 3. The bottom panels of Figure 3 show how this model (in black) compares with the observed TTVs (in red). This model does not represent a fit to the data; it merely demonstrates a realistic possibility for the TTVs.

While the observed transit times of "c" and "d" are consistent in amplitude with those predicted by the simple model, the statistically significant ∼2-minute deviations observed for K2-3b in the *Spitzer* data are not. The very low amplitudes of the model TTVs of "b" are due to the low masses of the perturbing planets, the wide separation between the "b" and the other planets, and the lack of proximity to low-order mean motion resonance.

To increase the amplitude to match the observations, our only truly unconstrained parameters are eccentricities and longitudes of pericenter, because the mass of "c" cannot be much larger than our estimated 5 $M_{\oplus}$ (a mass of ∼6.5 $M_{\oplus}$ results if the planet density was equal to that of iron). Larger-

Table 3
Transit Parameters Derived from Fits to the *Spitzer* Data

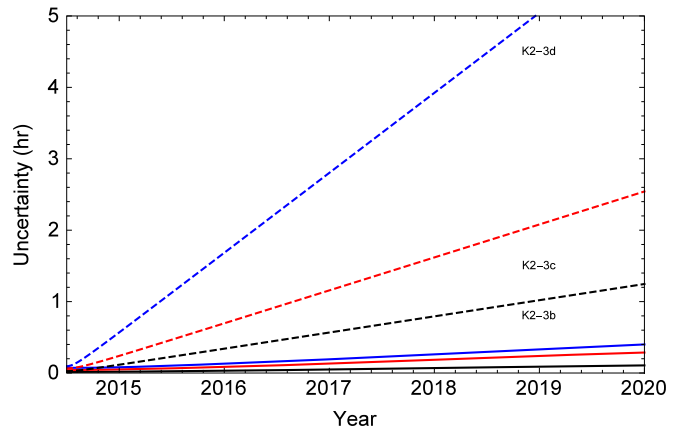| Parameter	Parameter	Parameter
Object	K2-3b (2015 Mar 13)	K2-3b (2015 Mar 23)
SMA/R_*	$29.60^{+1.44}_{-4.92}$	$30.43^{+2.68}_{-6.78}$
Incl (deg)	$89.71^{+1.03}_{-1.00}$	$89.31^{+1.25}_{-1.25}$
R_p/R_*	$0.0346^{+0.0007}_{-0.0007}$	$0.0371^{+0.0008}_{-0.0007}$
T0 (BJD)	$2{,}457{,}094.94852^{+0.00069}_{-0.00071}$	$2{,}457{,}105.00231^{+0.00061}_{-0.00071}$
Object	K2-3b (2015 Sep 15)	
SMA/R_*	$30.79^{+2.40}_{-7.10}$	
Incl (deg)	$90.19^{+1.20}_{-1.41}$	
R_p/R_*	$0.0341^{+0.0008}_{-0.0007}$	
T0 (BJD)	$2457275.92813^{+0.00091}_{-0.00069}$	
Period (*Spitzer* only)	10.0544403 ± 0.0000530 days	
Object	K2-3c (2015 Mar 26)	K2-3c (2015 Sep 6)
SMA/R_*	$51.12^{+5.81}_{-11.98}$	$50.71^{+4.55}_{-10.40}$
Incl (deg)	$89.98^{+0.89}_{-0.92}$	$89.86^{+0.80}_{-0.78}$
R_p/R_*	$0.0270^{+0.0008}_{-0.0007}$	$0.0271^{+0.0009}_{-0.0010}$
T0 (BJD)	$2{,}457{,}108.03149^{+0.00321}_{-0.00239}$	$2{,}457{,}280.55982^{+0.00217}_{-0.00211}$
Period (*Spitzer* only)	24.6469050 ± 0.0005002 days	
Object	K2-3d (2015 Mar 11)	K2-3d (2015 Sep 12)
SMA/R_*	$74.55^{+6.81}_{-11.99}$	$76.70^{+11.99}_{-17.95}$
Incl (deg)	$89.96^{+0.42}_{-0.44}$	$89.83^{+0.79}_{-0.74}$
R_p/R_*	$0.0240^{+0.0008}_{-0.0008}$	$0.0269^{+0.0008}_{-0.0007}$
T0 (BJD)	$2{,}457{,}093.57523^{+0.00356}_{-0.00502}$	$2{,}457{,}271.80073^{+0.00194}_{-0.00169}$
Period (*Spitzer* only)	44.5563737 ± 0.0011500 days	
Object	K2-26b (2015 Mar 12)	
SMA/R_*	$23.578193^{+1.580793}_{-3.422381}$	
Incl (deg)	$89.223181^{+1.063224}_{-1.039645}$	
R_p/R_*	$0.050253^{+0.001463}_{-0.001529}$	
T0 (BJD)	$2{,}457{,}168.503765^{+0.001777}_{-0.001801}$	

Figure 2. Dashed lines represent uncertainties in projected transit times (ignoring possible TTVs) based solely on *K2* data. Solid lines represent uncertainties from combined *K2* and *Spitzer* data. The colors correspond to K2-3b (black), K2-3c (red), and K2-3d (blue).

Schlieder et al. (2016) note the possibility that K2-26b might have a nonzero eccentricity based on its transit duration ($\epsilon > 0.14$; 2σ). The nonzero eccentricity, if real, may indicate past or present interactions with a perturbing body. With the current data, we find that the observed transit times do not show TTVs at any significance. However, this does not necessarily rule out a nearby perturbing planet, since the amplitude, timescale, and phase of a TTV signal depend on many unknown parameters.

4.3. Prospects for JWST Observing

The importance of objects like K2-3, with its system of three planets, is driven by the desire to carry out spectroscopic observations with *JWST* of planets in the size range of 1–2 $R_\oplus$. Such observations are possible for planets orbiting bright, late-type stars that yield a deep transit along with copious stellar photons to yield high(er)-S/N spectroscopy. Along with GJ 1214b, Kepler 138bcd, and the newly discovered GJ 1132b (Berta-Thompson et al. 2015), K2-3 represents a planetary system well suited for early *JWST* spectroscopic follow-up, at least until *TESS* targets become available. K2-3's planets have 1–2 $R_\oplus$, transit depths >100 ppm, and a host stellar magnitude [4.6 μm] $\leqslant 8.4$ mag. Indeed, K2-3 is almost a magnitude brighter than Kepler-138 (*WISE* [4.6 μm] < 9.4 mag). Situated in the HZ, K2-3d will allow study of a temperate ($\sim$300 K) mini-Neptune or super-Earth-sized planet.

We developed thermochemical equilibrium models and simulated *JWST* observations of the transmission spectra of several possible atmospheres for K2-3b and clear solar composition atmospheres of K2-3c and K2-3d using the

amplitude TTVs therefore require the orbits of "b" and "c" to be eccentric. However, since planet "c" interacts much more strongly with planet "d" than it does with "b," because the semimajor axis ratio is smaller between this pair compared with the (b, c) pair, this scenario would predict larger TTVs for "c" and "d" compared with those of "b."

In summary, we find tantalizing evidence for TTVs for K2-3b between *K2* and *Spitzer* epochs. The TTV amplitudes predicted for a configuration with nearly circular orbits and realistic masses is low enough to be consistent with a null detection of TTVs. More observations are required to assess whether TTVs of a few minutes seen in the combined *K2* plus *Spitzer* data for planet "b," which are marginally significant ($\sim$2σ) at this stage, are in fact reflective of stronger dynamical interactions.

Table 4
Ephemeris Parameters from Combined *K2* and *Spitzer* Transits

Planet	T0 (BJD)	Period (days)	$\Delta T0/\sigma$[a]	ΔPeriod$/\sigma$[a]
K2-3b	$2{,}456{,}813.42024 \pm 0.00094$	10.054544 ± 0.000029	0.93	2.0
K2-3c	$2{,}456{,}812.2777 \pm 0.0026$	24.64638 ± 0.00018	-0.25	0.74
K2-3d	$2{,}456{,}826.2248 \pm 0.0038$	44.55765 ± 0.00043	0.29	-0.92
K2-26b	$2{,}456{,}775.16503 \pm 0.00050$	14.568101 ± 0.000020	-0.09	0.88

Note.
[a] Differences in T0 and period from *K2*+*Spitzer* to *K2*-only values from Table 1 relative to combined uncertainties.

Table 5
Comparison of Planet/Star Ratio

Planet[a]	*Kepler*	*Spitzer*	Diff/sigma	*Kepler+Spitzer*
K2-3b Epoch1 + 2				
R_p/R_*	0.03483 ± 0.00097	0.0353 ± 0.0011	0.29	0.0350 ± 0.0007
$R_p/R_\oplus$				2.08 ± 0.25
K2-3c				
R_p/R_*	0.027 ± 0.001	0.02705 ± 0.00005	0.04	0.0270 ± 0.0006
$R_p/R_\oplus$				1.69 ± 0.21
K2-3d				
R_p/R_*	0.0250 ± 0.0016	0.02545 ± 0.0005	0.28	0.0252 ± 0.0007
$R_p/R_\oplus$				1.61 ± 0.20
K2-26b				
R_p/R_*	0.0471 ± 0.0028	0.0412 ± 0.0022	1.66	0.0434 ± 0.0017
$R_p/R_\oplus$				2.47 ± 0.40

Note.
[a] Assumes $R_* = 0.561 \pm 0.068\ R_\odot$ for K2-3 (Crossfield et al. 2015) and $R_* = 0.52 \pm 0.08\ R_\odot$ for K2-26. (Schlieder et al. 2016).

Table 6
Central Transit Times for K2-3b

Obs.	Orbit	BJD[a]	Obs.	Orbit	BJD[a]	Obs.	Orbit	BJD[a]
		K2-3b			K2-3b			K2-3b
K2	0	1980.4182 ± 0.0015	*K2*	0	1979.2785 ± 0.0026	*K2*	0	1993.2229 ± 0.0039
K2	1	1990.4744 ± 0.0016	*K2*	1	2003.9288 ± 0.0028	*K2*	1	2037.7829 ± 0.0049
K2	2	2000.5259 ± 0.0016	*K2*	2	2028.5722 ± 0.0037	*Spitzer*	6	2260.5752 ± 0.0043
K2	3	2010.5817 ± 0.0017	*K2*	3	2053.2151 ± 0.0047	*Spitzer*	10	2438.8007 ± 0.0018
K2	4	2020.6334 ± 0.0017	*Spitzer*	12	2275.0315 ± 0.0028			
K2	5	2030.6876 ± 0.0018	*Spitzer*	19	2447.5598 ± 0.0021			
K2	6	2040.7443 ± 0.0020						
K2	7	2050.7972 ± 0.0017						
Spitzer	28	2261.94852 ± 0.00070						
Spitzer	29	2272.00231 ± 0.00066						
Spitzer	46	2442.92813 ± 0.00079						
	$\chi^2 = 23$ with 9 dof[b]			$\chi^2 = 3.4$ with 4 dof			$\chi^2 = 1.4$ with 2 dof	

Notes.
[a] BJD–2,454,833.
[b] The χ^2 statistic for the hypothesis of a simple model with a constant period.

techniques employed by Greene et al. (2016). Clear solar composition, cloudy solar, and 100% H_2O atmospheres were generated for K2-3b, and we used the CHIMERA forward model (Line & Yung 2013; Line et al. 2013) and Kreidberg et al. (2014a, 2014b) to generate the transit transmission spectra for all planetary atmospheres over 1–11 μm. We simulated *JWST* NIRISS SOSS (1–2.5 μm), NIRCam grism (2.5–5.0 μm), and MIRI LRS (5.0–11 μm) transmission spectra of the three planets in the K2-3 system using the techniques described in Greene et al. (2016). The resultant spectra include photon, background, detector, and systematic noise components. They were binned to spectral resolving power $R = 35$ and are shown in Figure 4. Noise levels were set by a combination of photon noise and a floor set by residual detector artifacts. We adopted 18 ppm noise floors for NIRISS and NIRCam and 30 ppm for MIRI's longer-wavelength detectors (Beichman et al. 2014). The single transit measurement for K2-3b has a total noise level between around 23 and 30 ppm at wavelengths less than 4 μm. The K2-3c and 3d simulations are for five transits, so that the noise floor dominates with total

noise 19–25 ppm from 1 to 5 μm before jumping up to 34–44 ppm at MIRI wavelengths.

Figure 4 shows that *JWST* should detect strong H_2O (e.g., 1.4 μm) and the strong 2.3, 3.4, and 7.7 μm CH_4 molecular features in the clear solar atmosphere models. Combining the information in a complete 1–11 μm spectrum (observed in three or four transits total) of K2-3b would allow distinguishing between clear solar and cloudy or high mean molecular weight (e.g., pure H_2O) atmospheres for that planet. More than one transit may need to be observed at each wavelength in order to measure the mixing ratios of detected molecules with moderate precision (better than 1 dex) if K2-3b does not have a totally clear solar composition atmosphere. Spectra from several transits will need to be co-added to detect these features individually in clear solar atmospheres for K2-3c and K2-3d.

5. CONCLUSIONS

We have used the *Spitzer Space Telescope* to observe transits of the three planets orbiting the M0 star EPIC 201367065 (K2-3b, c, d) and one planet orbiting the M star EPIC 202083828
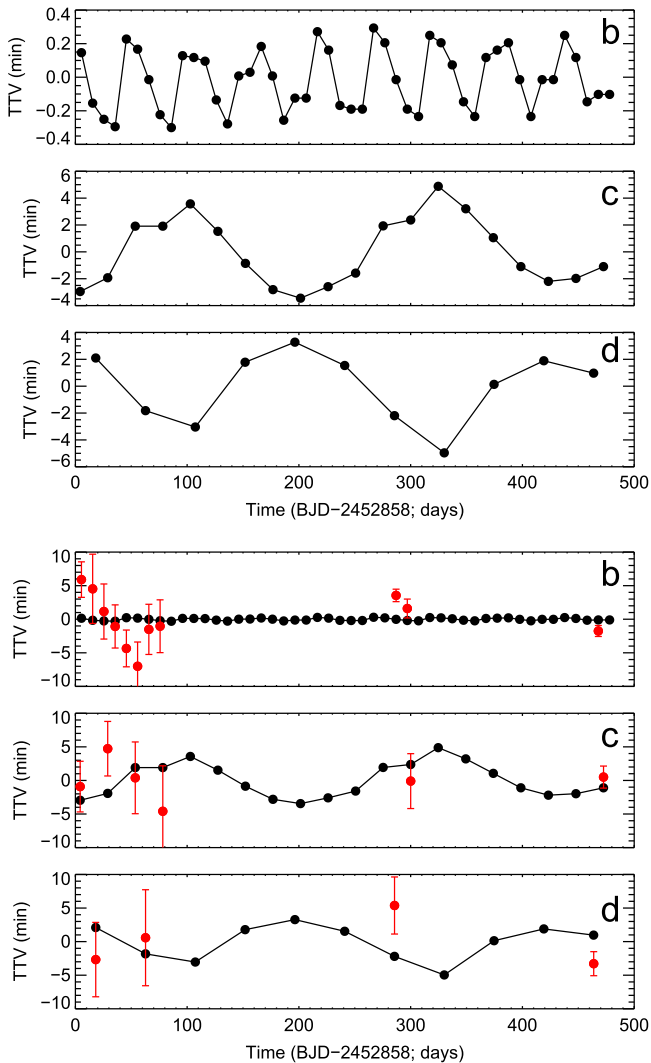
Figure 3. Top: predicted TTVs for the three planets orbiting K2-3 based on an illustrative model assuming circular orbits and nominal masses. Each sub-panel is labeled with the name of the planet (b, c, d). The predicted TTVs for K2-3b are only a fraction of a minute, much smaller than the observed deviations. Deviations for the outer planets could be as large as 5–10 minutes, but are not constrained by these data. Bottom: same models but with the data overplotted on an expanded scale.

(K2-26). The results allow us to refine the parameters of these planetary systems and greatly improve the precision of the ephemerides in support of future observations, notably with *JWST* for spectroscopic follow-up. The observations have reduced the uncertainties in predicted transits of K2-3 planets from 4–6 hr down to less than 1 hr. For K2-26b, the observations provide strong support for the exoplanet nature of the transiting object by eliminating a number of false positives.

Predicted spectra for the K2-3 planets suggest that *K2* will provide *JWST* with planets straddling the super-Earth to mini-Neptune classes suitable for spectroscopic characterization early in *JWST*'s mission.

These observations represent just the initial results of a larger *Spitzer* program that will improve the ephemerides, search for TTVs, and, in some favorable cases, provide observations of secondary eclipses.
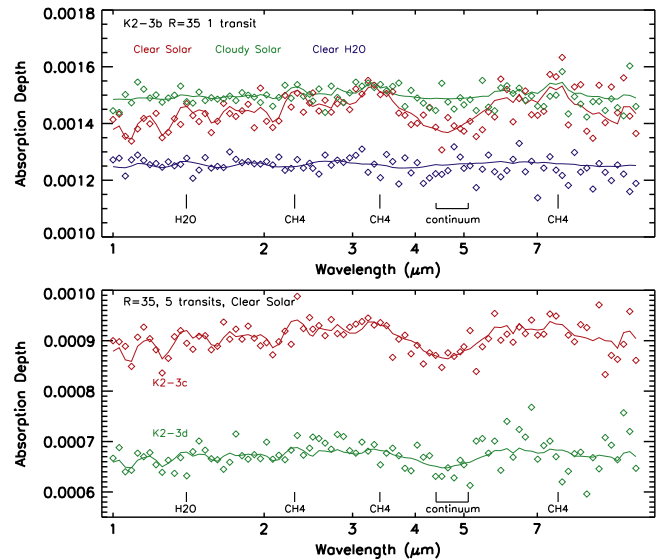
Figure 4. Top: model and simulated *JWST* NIRISS SOSS, NIRCam grism, and MIRI LRS transmission spectra of K2-3b, adapted from Greene et al. (2016). Model atmospheres binned to $R = 35$ are shown as solid curves, and the simulated data points (diamonds) were drawn from a Gaussian noise distribution for a single 2.3 hr transit plus an equal amount of time on the star at each wavelength. Photon noise and a systematic noise floor of 18 ppm ($1 \leqslant \lambda \leqslant 5\ \mu$m; NIRISS and NIRCam) or 30 ppm ($\lambda > 5\ \mu$m) were included in the total noise estimate. Bottom: similar models for planets K2-3c and d with data co-added for five transits at each wavelength. In both cases, a complete spectrum of the entire 1–11 μm wavelength region will require observations of three or four transits with different instrument modes to obtain one transit at each wavelength. Strong features of H_2O, CH_4, and a clear continuum region are indicated.

REFERENCES

Almenara, J. M., Astudillo-Defru, N., Bonfils, X., et al. 2015, A&A, 581, L7
Batalha, N., Mandell, A., Kalirai, J., & Clampin, M. 2014, in Search for Life beyond the Solar System. Exoplanets, Biosignatures & Instruments, 3
Beichman, C., Benneke, B., Knutson, H., et al. 2014, PASP, 126, 1134
Beichman, C., Ciardi, D., Akeson, R., et al. 2013, arXiv:1309.0918

Berta-Thompson, Z. K., Irwin, J., Charbonneau, D., et al. 2015, Natur, 527, 204

Carter, J. A., Agol, E., Chaplin, W. J., et al. 2012, Sci, 337, 556

Claret, A., & Bloemen, S. 2011, A&A, 529, A75

Crossfield, I. J. M., Petigura, E., Schlieder, J. E., et al. 2015, ApJ, 804, 10

Deck, K. M., & Agol, E. 2015, ApJ, 802, 116

Deck, K. M., Agol, E., Holman, M. J., & Nesvorný, D. 2014, ApJ, 787, 132

Deming, D., Knutson, H., Kammer, J., et al. 2015, ApJ, 805, 132

Désert, J.-M., Charbonneau, D., Torres, G., et al. 2015, ApJ, 804, 59

Dressing, C. D., & Charbonneau, D. 2013, ApJ, 767, 95

Dressing, C. D., & Charbonneau, D. 2015, arXiv:1501.01623

Evans, T. M., Aigrain, S., Gibson, N., et al. 2015, MNRAS, 451, 680

Fazio, G. G., Hora, J. L., Allen, L. E., et al. 2004, ApJS, 154, 10

Foreman-Mackey, D., Hogg, D. W., Lang, D., & Goodman, J. 2013, PASP, 125, 306

Goodman, J., & Weare, J. 2010, Comm. Appl. Math and Comp. Sci, 5, 65

Greene, T. P., Line, M. R., Montero, C., et al. 2016, ApJ, 817, 17

Grillmair, C. J., Carey, S. J., Stauffer, J. R., et al. 2012, Proc. SPIE, 8448, 84481I

Howard, A. W., Marcy, G. W., Bryson, S. T., et al. 2012, ApJS, 201, 15

Howell, S. B., Sobeck, C., Haas, M., et al. 2014, PASP, 126, 398

Ingalls, J. G., Krick, J. E., Carey, S. J., et al. 2012, Proc. SPIE, 8442, 84421Y

Knutson, H. A., Dragomir, D., Kreidberg, L., et al. 2014, ApJ, 794, 155

Knutson, H. A., Lewis, N., & Fortney, J. J. 2012, ApJ, 754, 22

Kreidberg, L., Bean, J. L., Désert, J.-M., et al. 2014a, ApJL, 793, L27

Kreidberg, L., Bean, J. L., Désert, J.-M., et al. 2014b, Natur, 505, 69

Krick, J., Ingalls, J. C., Grillmair, S., et al. 2015, IRAC High Precision Photometry Website, http://irachpp.spitzer.caltech.edu

Line, M. R., Wolf, A. S., Zhang, X., et al. 2013, ApJ, 775, 137

Line, M. R., & Yung, Y. L. 2013, ApJ, 779, 3

Mazeh, T., Nachmani, G., Holczer, T., et al. 2013, ApJS, 208, 16

Mordasini, C., Alibert, Y., Benz, W., Klahr, H., & Henning, T. 2012, A&A, 541, A97

Parviainen, H. 2015, MNRAS, 450, 3233

Payne, M. J., & Lodato, G. 2007, MNRAS, 381, 1597

Ricker, G. R., Winn, J. N., Vanderspek, R., et al. 2014, Proc. SPIE, 9143, 914320

Schlieder, J. E., Crossfield, I. J. M., Petigura, E. A., et al. 2016, ApJ, 818, 87

Skrutskie, M. F., Cutri, R. M., Stiening, R., et al. 2006, AJ, 131, 1163

Steffen, J. H., Fabrycky, D. C., Agol, E., et al. 2013, MNRAS, 428, 1077

Sullivan, P. W., Winn, J. N., Berta-Thompson, Z. K., et al. 2015, ApJ, 809, 77

Weiss, L. M., & Marcy, G. W. 2014, ApJL, 783, L6

Werner, M. W., Roellig, T. L., Low, F. J., et al. 2004, ApJS, 154, 1

Wong, I., Knutson, H. A., Lewis, N. K., et al. 2015, ApJ, 811, 122

Wright, E. L., Eisenhardt, P. R. M., Mainzer, A. K., et al. 2010, AJ, 140, 1868